ABSTRACT

JANAGARAJAN KALAIVANI, GOUSHIKA JANANI. Haptic Feedback for Virtual Reality Therapy. (Under the direction of Drs. Derek G. Kamper and Alexander Dean).

Hand rehabilitation in stroke survivors requires extensive repetitive practice. Most of the stroke survivors give up therapy, however, due to disengagement and boredom arising from monotonous repetition[1]. Virtual reality (VR) may improve engagement. Over 85% of participants in one study found VR based rehabilitation to be effective in encouraging them to practice repetitive movements [2]. VR games have additional appeal, in that they can be customized to the difficulty level appropriate for a given user at a given time and can thus provide personalized care. Maintaining an appropriate level of challenge is key for motor learning [3]. Finally, VR interventions can be cost-effective.

Hand impairment is one of the most common stroke outcomes [4]. The level of impairment may preclude voluntary practice. Thus, hand exoskeletons have been developed to facilitate the practice of hand movements by helping to complete the intended motion. Hand exoskeletons offer an additional potential benefit when they are used in conjunction with VR systems; they offer a means of increasing sensory feedback through haptics. This is especially important for the hand, which relies so heavily on sensory input for task performance.

The goal of this study was to adapt a hand exoskeleton to provide haptic feedback to users of a VR rehabilitation environment. Detection of interaction with specific objects in the VR environment triggered a corresponding production of haptic force in the exoskeleton, the X-Glove. Communication between the exoskeleton and VR environment was achieved through Bluetooth low energy protocol. Haptic feedback in the X-Glove, was achieved through impedance control with force feedback. The performance of P and PID controllers revealed that the PID controller was more accurate and robust to noise than the P controller. During

simulation of a stiffness of 0.67 N/mm, the root mean square error (RMSE) for the PID compensator was 77.63% less than that of the P controller.

Haptic Feedback for Virtual Reality Therapy

by
Goushika Janani Janagarajan Kalaivani

A thesis submitted to the Graduate Faculty of
North Carolina State University
in partial fulfillment of the
requirements for the degree of
Master of Science

Electrical Engineering

Raleigh, North Carolina
2020

APPROVED BY:

_____	_____
Dr. Derek Kamper	Dr. Alexander Dean
Committee Co-Chair	Committee Co-Chair

_____
Dr. Edward Grant

BIOGRAPHY

I received my Bachelor of Engineering in Electronics and Communication Engineering from College of Engineering Guindy, Anna University in 2016 graduating Cum Laude. After graduation, I joined Caterpillar India Private Limited as an Associate Engineer developing and testing software for controllers. I desired to gain more engineering experience to solve problems with unique approaches. I joined graduate school at North Carolina State University in 2018 to pursue a Master's in Electrical Engineering.

ACKNOWLEDGMENTS

I would like to thank my P.I. Dr. Derek G. Kamper for taking me in his lab and giving me this project. Many thanks to his guidance and patient clarifications. I thank James McCall for guiding my research works in the Hand Rehabilitation Lab and proof-reading my thesis drafts and presentation. Thank you James Ailsworth for helping me to build a fixture for a validation test setup. Many thanks to Mohammad Ghassemi for helping me in this project whenever I am lost and could not proceed further.

I would like to extend my thanks to Dr. Alexander Dean, who gave me unique approaches in embedded programming. I thank my other wonderful committee member Dr. Edward Grant for his help in debugging the system.

Very special gratitude to my uncle, Mohanraja for inspiring me to do research. As ever, I thank my mom, Kalaivani and dad, Janagarajan for supporting my decision to enter graduate school in the United States. I am indebted to their love, prayers and blessings.

TABLE OF CONTENTS

LIST OF TABLES

LIST OF FIGURES

CHAPTER 1: INTRODUCTION

1.1 Stroke Incidence

Stroke occurs when blood flow to part of the brain is restricted due to a clogged artery (ischemic stroke) or a ruptured artery (hemorrhagic stroke). Roughly 87% of strokes are ischemic, and 13% are hemorrhagic [5]. Stroke is the fifth leading cause of death in the United States [6]. Nearly 800,000 incidents of new or recurrent stroke each year [5]. Most individuals will survive the stroke, thereby leading to over 7 million stroke survivors in the U.S. [5]. Unfortunately, the majority will have chronic impairment [7], especially of the hand; many stroke survivors experience difficulty with activities of daily living (ADLs), thus making stroke the leading cause of disability in the United States [6].

1.2 Typical Impairments

Impairments after stroke depend on the area of the brain which has been damaged. Common disabilities due to stroke are poor motor control, sensory disturbances, difficulty in using or understanding languages (aphasia), cognitive impairment, memory loss, and emotional disturbances [8].

1.2.1 Motor Control Impairments

Diminished muscle control and weakness (paresis) is a common outcome on one side of the body after stroke. This hemiparesis can affect facial expression, control of the arm or the leg, or all motor function on one side of the body, contralateral to the damaged hemisphere of the brain [8]. Weakness can be especially severe in the hand [9]. Grip strength can be reduced by more than 50% [10]. Weakness arises from multiple sources. Stroke survivors may exhibit reduced motor unit firing rates [11], which could contribute to the lack of voluntary muscle activation observed [12]. Altered muscle activation patterns may also contribute to the net

weakness [13], by leading to misdirected forces [14]. Excessive coactivation of antagonist muscles may also reduce net force generation. This coactivation seems to arise from involuntary hyperexcitability, apparent as spasticity [15] and prolonged muscle relaxation time [14].

1.2.2 Sensory Impairments

Loss of ability to feel touch, pain, temperature, or position can also occur after stroke [8]. Some individuals might experience severe sensory issues, essentially unable to feel their own limb. Damage to sensory pathways can result in transmission of false signals. Thalamic pain syndrome, for example, occurs when stroke damages the thalamus of the brain, which manages processing sensory information from brain to body. Pain may also arise from weakness that precludes joint movement for a prolonged period, thus leading to a 'frozen joint' situation. Stroke may especially impact touch sensation and proprioception [16]. This has a major impact on hand function due to the importance of sensory feedback to task performance with the hand [17].

1.3 Therapy Practices

The ability of the brain to reorganize its structure, function, and underlying connections in response to experiences is called neuroplasticity. Rehabilitative therapies are designed to exploit this remarkable potential of the brain. They aim to create new capabilities through repeated practice of selected tasks and movements. The goal of rehabilitation therapy is to make stroke survivors as independent as possible and to enable them to attain the best quality of life possible.

In the United States, the median length of stay of ischemic stroke patients in inpatient hospital care is 4 days [18]. All patients undergo a formal assessment of rehabilitation needs before discharge. Rehabilitation services are delivered by a multidisciplinary team of healthcare

providers in the fields of neurology, rehabilitation nursing, occupational therapy (OT), physical therapy (PT), speech and language therapy (SLT).

Upon discharge from the acute-care facility, stroke survivors requiring further rehabilitation will typically be transferred to either an intensive rehabilitation facility (IRF) or a skilled nursing facility (SNF). In an IRF, the patient is directly supervised by a physician and receives a minimum of 3 hours of therapy per day involving OT, PT, and/or SLT services as required by the patient for 5 days each week. At the SNF, rehabilitation care is directed by a physician, but directly administered by rehabilitation nurses.

Stroke survivors, after returning home, receive rehabilitation care either in the community by a home healthcare agency (HHCA) or through outpatient clinic visits. Throughout this recovery phase, an emphasis is placed on movement practice to promote self-care. These strategies may include adaptive techniques to employ the nonparetic side of the body to compensate for diminished control of the paretic side. While these compensatory techniques may lead to short-term benefits in helping the stroke survivor to return home sooner, they may inadvertently lead to further disuse of the paretic limbs. This underscores the importance of intensive practice with the paretic limb during therapy sessions. Therapies that can be extended into the home environment may provide further benefits.

Approximately 80% of over 6 million stroke survivors in the United States live in a community setting (home, board and care, transitional living, immediate care, or assisted living residence) with a majority of them living at home, but with some functional deficits [18]. This makes the study of rehabilitation therapies at home significant. Patient satisfaction is higher in home-based rehabilitation programs than in institutional care [19]. Besides, home-based programs offer reduced costs, along with greater flexibility for patient and family members'

involvement. This presents a possible means for stroke survivors living in remote areas to receive quality care. Over 66% of participants in a study showed interest in home therapy, and all study participants agreed to practice 2-3 times a week if home therapy were available [2].

1.4 Virtual Reality in Stroke Rehabilitation

Virtual reality (VR) refers to an advanced subset of computer games, which allows users to interact with a synthetic environment through multiple sensory (visual, auditory and/or haptic) channels [20]. The synthetic environments would be designed close to real-world objects/events with help of computer hardware and software. In VR games, the user can see his or her own movements in the simulated scene, thereby increasing the level of immersion. Several research groups [21]–[23] have examined at using VR in stroke therapy, and it is an emerging approach in stroke rehabilitation to encourage engagement in the clinic and at home. There are a number of advantages of using VR, such as 1) improved control of difficulty levels, thereby providing customized therapy practice 2) opportunities to practice real-world tasks in a safe environment and 3) cost-effectiveness [24]. Repetitive movement is critical to attainment of lasting functional behaviors [25], but most stroke survivors give up therapy before witnessing optimal results due to lack of motivation, disengagement and boredom [1]. VR games, with their engaging nature, may fulfill the conditions leading to neuroplasticity such as high repetitions, intensity, and task-oriented training of the paretic side [26]. Over 85% of participants in one VR game study found such games to be effective in promoting repetitive arm movements [2].

1.5 Haptics and Virtual Reality in Upper Extremity Rehabilitation

Sensation plays a significant role in hand movement in healthy individuals, e.g., reaching into a pocket to pull out the desired coin. Thus, sensation is important for rehabilitation. Incorporating sensory feedback into VR therapy helps to maximize effectiveness of the

treatment. Haptic devices are designed to provide feedback to two key somatosensory systems, namely kinesthetic and cutaneous systems. The devices that target kinesthetic system provide force feedback to assist, perturb hand movements. Tactile devices may use vibration, pressure, or temperature to convey cutaneous information.

Evidence in healthy individuals shows the benefits of using VR with haptics over VR alone in certain tasks affecting completion time and accuracy [27]. One study confirmed that cortical reorganization occurred in stroke survivors after participating in haptic enabled therapy by examining brain activation through functional magnetic resonance imaging [28]. Another study found a high user acceptance rate in haptic enabled therapy [29]. Significant positive results of using haptics were also seen in the multiple sclerosis population [30]. The idea of using haptics to trigger plasticity in somatosensory regions of the brain in stroke survivors and the role of haptics in improving motor control are potential areas for research. A previous study [28] looked at providing haptics with a robot. I propose to integrate haptics into a custom VR environment using a custom hand exoskeleton.

1.6 Project Overview

The goal of this study was to integrate an existing hand exoskeleton, the eXtension (X)-Glove, with a custom virtual reality environment to enable therapy with haptic feedback for stroke survivors. The X-Glove [31] is an actuated glove controlled by a Pic32 microcontroller. The X-Glove can actuate each digit independently while also allowing free rotation of joints. Utilizing the position and force sensors in each digit, I created an impedance controller to simulate objects of different levels of stiffness. In particular, I compared the effectiveness of proportional (P) versus proportional-integral-derivative (PID) controllers. Additionally, I utilized the Bluetooth Low Energy (BLE) protocol to provide communication between the

exoskeleton and the virtual reality software, running in the Unity 3D environment. Finger displacements provided by the X-Glove are combined with hand location data obtained from a motion capture system to determine object contact with the virtual environment. The associated object stiffness values are then transmitted from the VR computer back to the X-Glove to create the target haptic force. Fingertip force is used to update the virtual scene by representing associated object deformation.

The rest of the thesis is arranged in the following manner. Chapter 2 provides an overview of the system setup. Chapter 3 describes the methods employed to achieve the goal of the study. Chapter 4 describes results and discussion. This is followed by the conclusions in Chapter 5.

CHAPTER 2: SYSTEM DESCRIPTION

This study focused on the integration of an existing hand exoskeleton, the X-Glove, with a custom virtual reality exercise created in the Unity environment.

2.1 Exoskeleton

This study used a prototype of a device developed in the Hand Rehabilitation Lab. This prototype (**Figure 1**) represents an improved version of the X-Glove, which has been employed in a number of previous studies with stroke survivors [31].

The device consists of a glove actuated by linear servomotors (Actuonix Motion Devices Inc., Victoria, BC, Canada; model L12 micro linear actuator). Each of the five servomotors independently actuates one digit and is capable of producing both digit flexion and digit extension. Movement of the motor pulls or pushes the cable, thereby causing joint rotation. Force is transmitted from the linear servomotor to the digit through a flexible cable. Pushing with the cable is possible due to the guides used to direct the cable. Rigid cable guides attached to the glove direct the cable pathway, prevent joint hyperextension, and maintain moment arms. Flexible guides between the rigid guides prevent buckling during pushing.

Sensors on the glove provide feedback for each digit. Cable position (and thus finger displacement) is measured by quantizing the analog position feedback signal from a potentiometer in the servomotor. A load cell (Forsentek Co., China; model L13B) placed in series with the actuator measures force for each finger and for the thumb.

The X-Glove is designed to be portable. A control unit is positioned on the upper arm. The controller board is comprised of Pic32 microcontroller (Microchip Technology Inc., Chandler, US; model Pic32MX795), Bluetooth module (Silicon Labs, Austin, US; model BLE 113), analog to digital converter (ADC) (Analog Discovery Inc., Norwood, US; model

LTC1859), digital to analog converter (DAC) (Maxim Integrated, San Jose, US; model MAX5307), OLED display and custom power conditioning circuit (**Figure 2**). The Pic32 is a powerful microcontroller for embedded control applications with peripherals like Timer, USART, and SPI. A timer was used in the synchronous sampling of sensor input and output at 1 kHz. USART was used in the communication between the Pic32 microcontroller and the BLE 113 module. SPI communication protocol was followed to establish communication between the Pic32 and the ADC.

The LTC1859 module is used instead of the ADC peripheral native due to the constraints of Pic32 ADC unit. The native ADC unit has an input range of 0 to 3.3V. The load cell output runs between 0 and 5V. Hence, a separate ADC is being used instead of the built-in peripheral of Pic32. Also, the native unit does not have enough ADC input channels for the 5 load cell signals and 5 motor position signals. The LTC1859 provides 16-bit resolution. MAX5307 module is a 12 bit DAC. It delivers position input signal between 0 and 5V for the linear actuator.

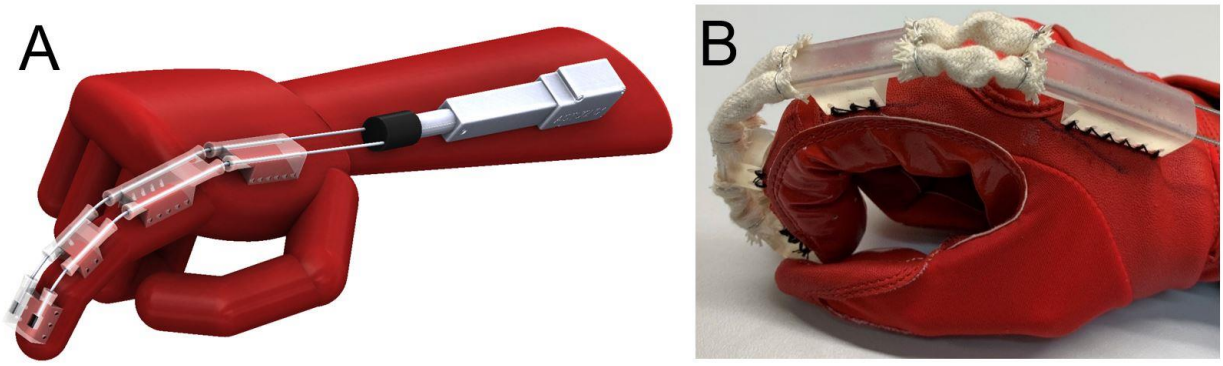

Figure 1. X-Glove Prototype. X-Glove assembly for index finger actuation is shown in the figure. (A) 3D model. (B) Flexible cotton sleeves are present between rigid guides.

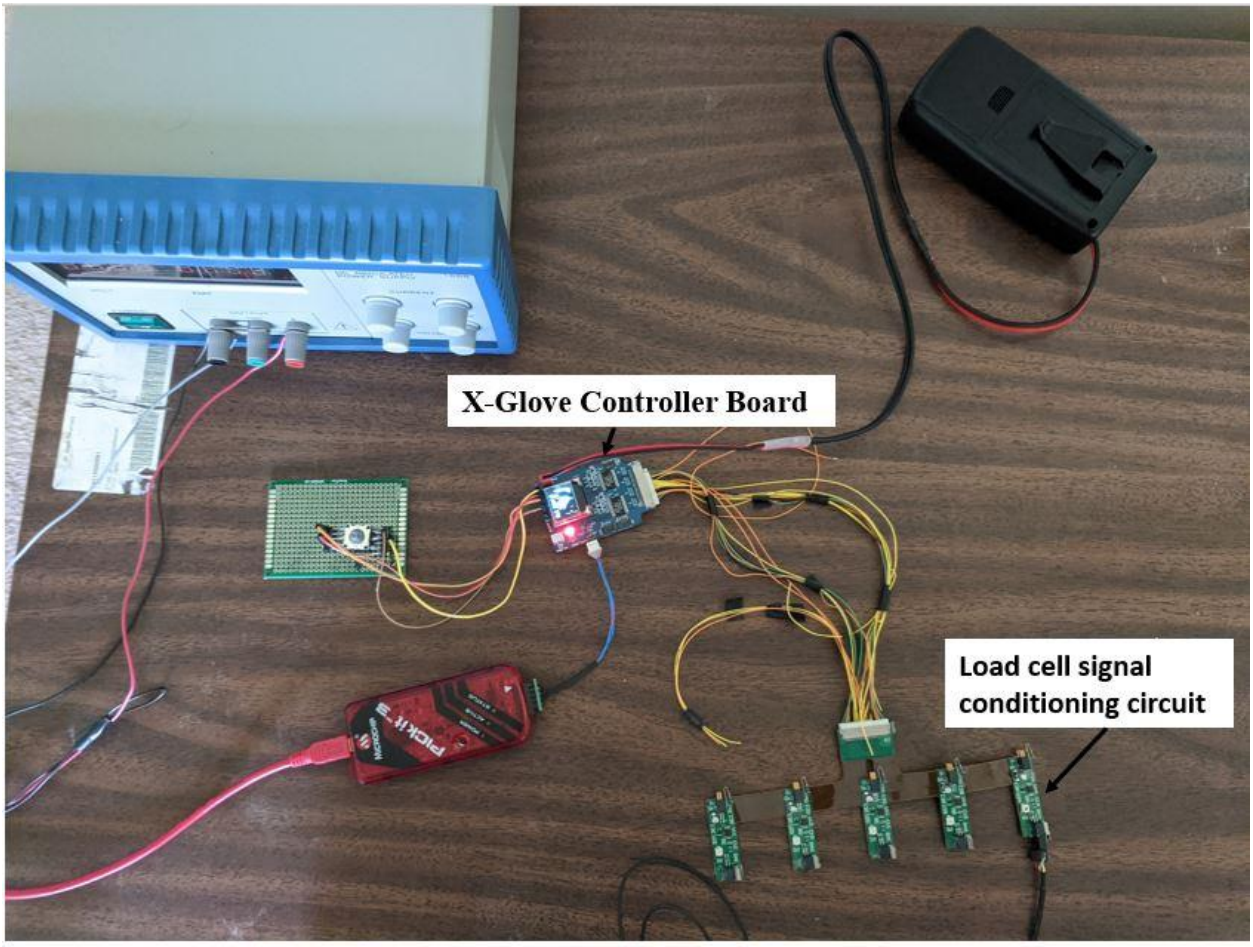

Figure 2. X-Glove Components. Electrical components that support the control of the X-Glove.

2.2 Software Development Tool

MPLAB X IDE (Microchip Technology Inc., Chandler, US; version 5.20) with xc32 (Microchip Technology Inc., Chandler, US; version 2.0) toolchain was used to develop, debug the embedded C code for the Pic32. The code was developed in MPLAB Harmony (Microchip Technology Inc., Chandler, US; version 2.06) software framework. Pickit3 debugger (Microchip Technology Inc., Chandler, US) was used to flash and debug code to the Pic32 microcontroller. The VR game was developed in C# in Microsoft Visual Studio, which is integrated with the Unity game engine. For data processing and visualization, Matlab 2019b (MathWorks, Natick, US) was used.

2.3 Virtual Reality Environment

Virtual reality environment used in this study is a custom kitchen (**Figure 3**) where participants can interact with a variety of food objects, either passing them back and forth for engaging in a Foodfight game [1], [2]. The environment runs in Unity 3D (Unity (Unity Technologies, San Francisco, US; version 2018.4.19f1). Each participant is represented as an avatar. Movement of the user produces corresponding movement of the avatar segment. User movements are measured with Kinect motion capturing system (Microsoft Corp., Redmont, USA; model version 2). These data are transmitted via the UDP protocol to the computer that runs the VR game. Multiple users can interact within the same environment.

Figure 3. VR Game Scene. Two users play the VR Foodfight game that promotes hand movements by grabbing and throwing game objects in the VR scene.

CHAPTER 3: METHODS

Modifications were performed to improve the capabilities of the exoskeleton, the virtual reality environment, and the communication between them. The new system was employed to institute haptic feedback. These modifications and the experimental set-up used to test and evaluate control are described in this chapter.

3.1 Hand Exoskeleton

3.1.1 Load cell Calibration

As noted, the X-Glove contains load cells connected in series with the cables and servomotors. In order to simulate absolute stiffness, calibration of these load cell values as they appear in the microcontroller was required. The output signal from the load cell is first conditioned in analog electronics. The signal is filtered with a first order lowpass filter of cut-off frequency of 36 Hz and passed through an instrumentation amplifier with a gain of 910. A potentiometer located on the signal conditioning board (**Figure 2**) was adjusted to remove any voltage offset in the circuit.

The signal is then sampled and converted to a 16-bit digital value using the LTC1859 ADC module on the X-Glove controller board. The ADC communicated with the Pic32 microcontroller via SPI (Serial Peripheral Interface) protocol. Maximum conversion time of the ADC is 5 μs . A timer interrupt handler issues an ADC conversion request every 1 ms via SPI protocol. The conversion request is a byte data containing information about the ADC channel and input range before every conversion. Simultaneously, the output of the previous conversion is made available in the Serial Data Output (SDO) line, as SPI is a data exchange protocol. Hence, there is one ADC read delay between conversion request and the ADC output (**Figure 4**).

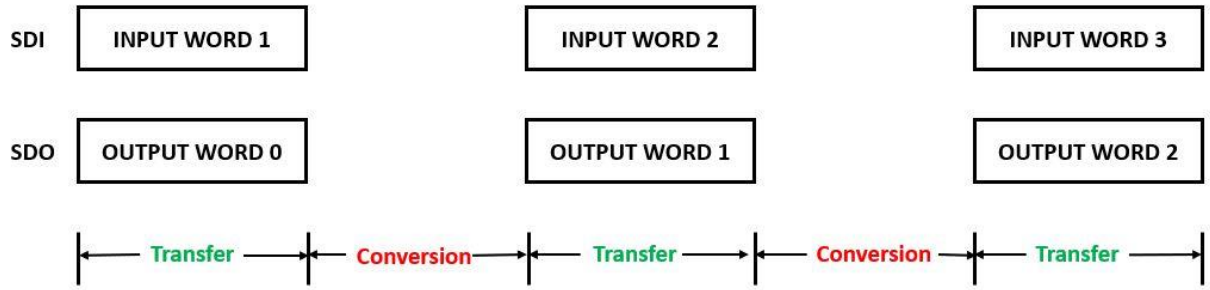

Figure 4. Data exchange mechanism of the ADC. Synchronous data transfer to and from ADC occurs in SDI and SDO data lines, respectively.

To find the linear relationship between the digital value and force in N, different known forces were applied using a spring scale (Etekcity Corp., California, US; model EHS18). The corresponding digital value was lowpass filtered using a second-order Butterworth filter of cut-off frequency 0.5 Hz in Matlab (**Table 1**). Linear regression was subsequently used to fit a model between the known force in N and the representative value in Data Acquisition (DAQ) counts (**Eqn 3.1**). The actual data were well modeled by the linear approximation (**Figure 5**), with root mean square error (RMSE) of 120.45 DAQ counts, or 1.9 % of the DAQ count for 3 kg.

$$Force\ DAQ\ Counts = 251.46N - 859.32 \quad (3.1)$$

Table 1. Load Cell Calibration Data

Mass (g)	**Force** (N)	**DAQ Counts**
580	5.68	500
1130	11.07	2000
2000	19.6	4000
2500	24.5	5500
3000	29.4	6400

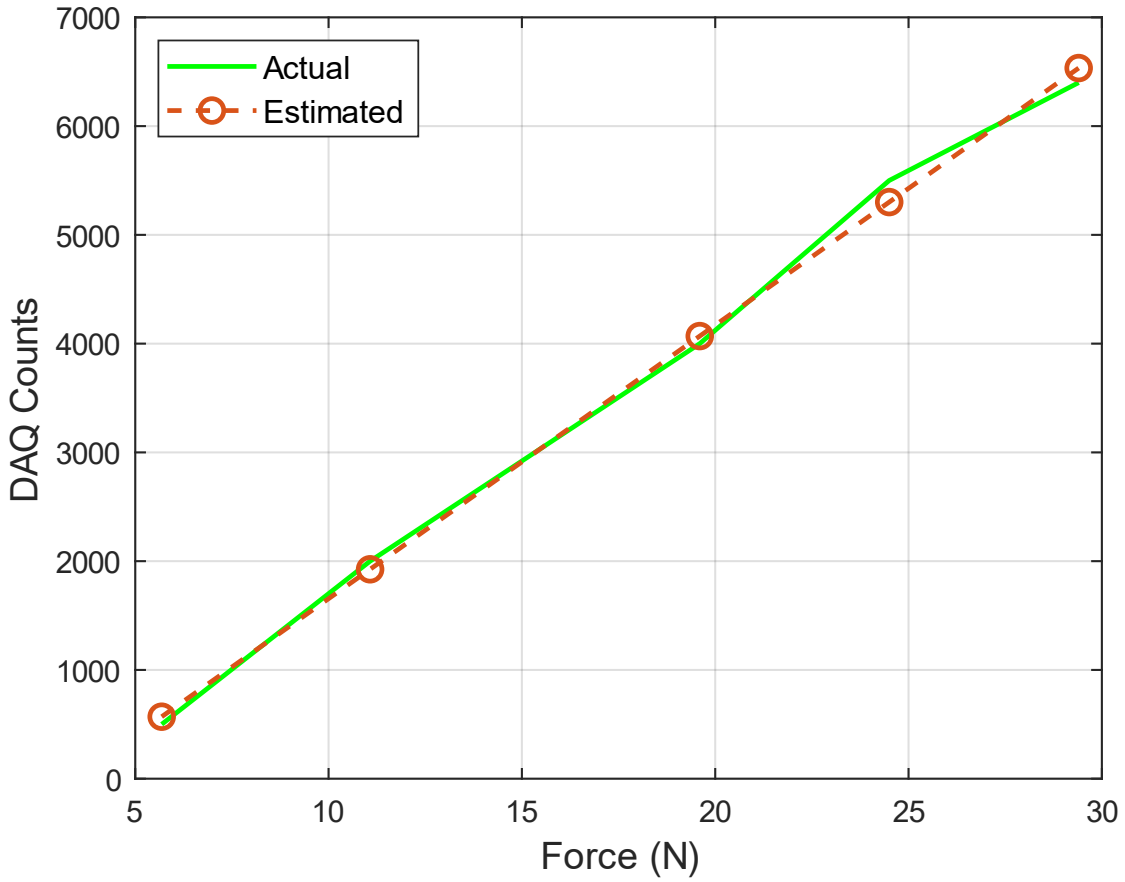

Figure 5. The relationship between DAQ counts and N. Data of known forces in N and corresponding ADC converted values were fit in a first-order polynomial equation.

3.1.2 Motor Position Data

The linear actuator has an onboard non-programmable digital position controller. The position information is available as a proportional voltage signal between 0 and 3.3 V from the servomotor. This voltage signal was sampled and converted into a 16-bit value. The stroke length of the actuator is 50 mm. Measurements were taken to relate the motor position in mm and its digitized value (**Table 2**). A linear relationship was estimated (**Eqn. 3.2**). The actual and estimated values (**Figure 6)** were found to have a RMSE of 204.3 DAQ Counts. The polynomial coefficients of the linear relationship in descending powers were -778, 42765. They were calculated by fitting data with least square error.

$$Motor\ Position\ DAQ\ Count = -778 stroke\ length\ (mm) + 42765 \qquad (3.2)$$

Table 2. Digitized Stroke Length Data

Stroke Length (mm)	**DAQ Counts**
13	33350
25	23520
37	13760
50	3900

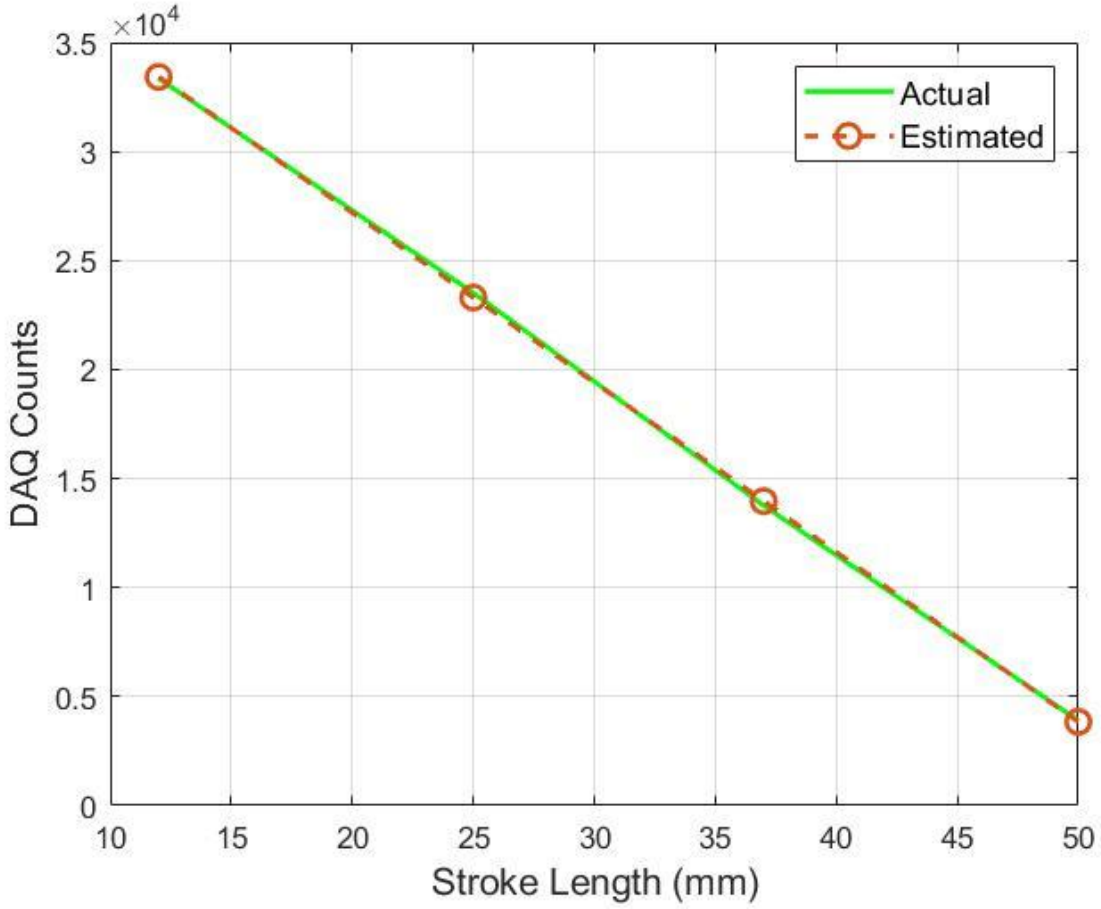

Figure 6. Relationship between stroke length(mm) and digital value. The linear relationship between stroke length of the actuator and ADC digital value was estimated using polyfit function in Matlab.

3.2 VR Environment

This study utilized a custom VR exercise, created using the Unity game engine, to create haptic feedback for the user when a virtual object is "grasped". This exercise consists of grasping food objects present in the game scene and either passing them to or throwing them at the other participant. If the hand model of the avatar 'grasps' any of the game objects, an event to send haptic command is triggered. For this study, the exercise was modified to send the haptic

command on pressing a GUI button in the game scene display. This was done to speed up the testing process of the impedance controller in the X-Glove, which is the goal of the study.

3.2.1 Incorporation of Haptic Feedback

Each user controls an avatar which responds to the user`s movements. Motion of the head, torso, arms and legs is tracked with Kinect motion capturing sensors. The Kinect, however, does not provide adequate tracking of the hand digits. Instead, for this project a method was implemented to estimate fingertip motion from the motor position sensor data. Object contact was estimated from hand location, object location, object size, and fingertip position. Objects were modelled as spheres of known dimensions. Unity game engine detects collision when an avatar`s hand collides with a food object. Unity can track the position of each digit of the hand model. On colliding, if the distance between the thumb and any finger of the avatar`s hand becomes less than the size of the picked up object, the object is detected to be grasped.

Payload of the haptic command is stiffness of the game object and the fingers` position (length of the actuator). The payload is a 15 byte data containing 4 bytes for stiffness value of type float and 10 bytes for the position data of five fingers of type unsigned short, 1 byte for the haptic command identifier

3.2.2 Visualization of object deformation

Visual cues can supplement haptic feedback to improve motor learning. For example, observing the object deformation resulting from the force applied to a virtual object can inform the user about the appropriateness of chosen force levels. For this project, an initial object deformation scenario was incorporated.

Based on previous works that developed a jelly of variable stiffnesses that responded to mouse button clicks [32], [33], a jelly was created that responded to haptic forces. The jelly was modelled as a mesh, a collection of vertices that outline a surface. When pressure is applied on the surface, each vertex of the mesh acquires velocity. Force at each vertex F_v, is given by

$$F_v = \frac{F}{1+d^2}$$

where F is the contact force and d is the distance between the current vertex and the contact point. Force decreases with the square of the distance (adding 1 to d^2 allows maximum applied force F to occur at the contact point). In order to distribute force along the surface, an offset is added to the position of the contact point (**Figure 7**). This avoids the jelly to look as if it has been poked.

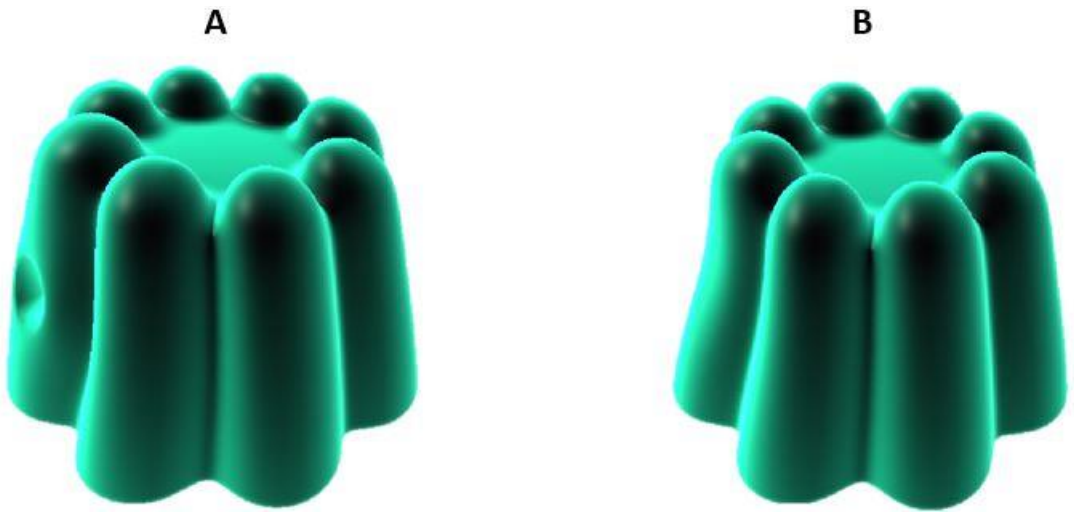

Figure 7. Effect of position offset. (A) Zero offset to the contact point applies force in all directions pushing vertices apart and causing a circular dent like appearance. (B) Using a positional offset of 30% lets the pressure to be distributed smoothly by pushing vertices into the surface.

The velocity of the mesh vertices depends on the stiffness factor. An invisible spring is modelled to connect the initial vertices and deformed vertices. Thus, the amount of deformation is determined by the spring force factor. To prevent infinite oscillation of spring, a damping factor is added to the model.

Two contact points were chosen on the left and right surfaces of the jelly. Force from a linear profile over time was applied to the points. This created an impact of squeezing by holding the jelly upright (**Figure 8B**). While simplistic, the equations for vertex velocity (see Appendix B) do produce relatively convincing visual effects.

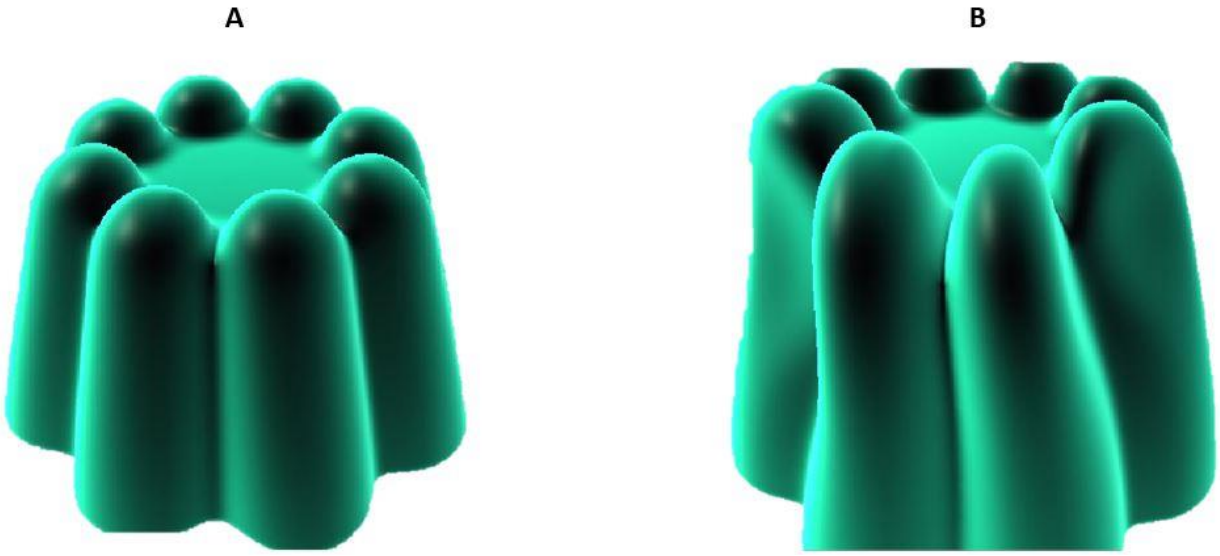

Figure 8. Jelly deformation. (A) The initial state of Jelly. (B) Deformed state of Jelly under pressure at two contact points on the periphery.

3.3 Communication

3.3.1 Wireless Data Transfer

Communication between the X-Glove and the VR environment is achieved for this project using the Bluetooth low energy (BLE) protocol. One Bluetooth transceiver, BLE 113 is

connected to the Pic32 microcontroller communicating over UART. Another Bluetooth transceiver BLED 112 (module (Silicon Labs, Austin, US) is connected to the VR computer that runs the Unity game engine. BLED 112 communicates with the computer via USB. BLE 113 is flashed with firmware to advertise itself for connection using CC Debugger (Texas Instruments, Dallas, USA)

The Pic32 application and the VR game are the host applications for the Bluetooth smart radio frequency (RF) stack of BLE 113 and BLED 112 modules respectively. The transport protocol between the host application and the Bluetooth stack is a simple command, response and event based protocol called BGAPI. BGLib is the parser for the BGAPI protocol and is included in the host applications. BGLib contains handlers for all BGAPI commands, responses and events and callbacks that help communication over UART (BLE 113) or USB (BLED 112).

The Bluetooth device has a database of attributes. Two attributes are created to exchange data between the X-Glove controller and the VR computer. One attribute is used to send length of the actuator from the X-Glove controller to the VR computer. This is sent to update the hand model in the VR game. Thus, it should be fast and data loss will not have much impact. Hence, it is made unacknowledgeable. Another attribute is used to send the haptic command from the VR game to the X-Glove controller. Data loss in this attribute is not acceptable. Hence, it is made acknowledgeable. Acknowledgements are received as events.

The BLE 113 module, that is connected to the X-Glove controller acts as the server. BLE 113 is configured to operate in “packet” mode and in the absence of flow control over UART. This mode enables DMA buffering and compensates for the data loss that might happen without using flow control.

The X-Glove and VR exercise must work in a highly coordinated manner to achieve haptic feedback (**Figure 9**). Displacement data from the fingertips and thumb are transmitted every 100 ms from the Pic32 to the VR computer. These data are used within the VR environment to determine if a virtual object is grasped. Importantly, the grasp aperture in the hand must be sufficiently large to permit grasp. This aperture can be individualized to the user to achieve the appropriate level of challenge. Once grasp contact is determined, the VR computer transmits information about the object stiffness K and the finger position at object contact x_t. The greater the squeezing or 'penetration' Δx ($\Delta x = x - x_t$), the higher the haptic force that the user should experience. By sending the fingertip location at the time of contact rather than the desired force to the hand exoskeleton, better fidelity in haptic control can be achieved as delays are reduced. Once the X-Glove receives a signal from the VR computer that contact has been made, it initiates impedance control according to the object stiffness and fingertip displacement from the threshold x_t.

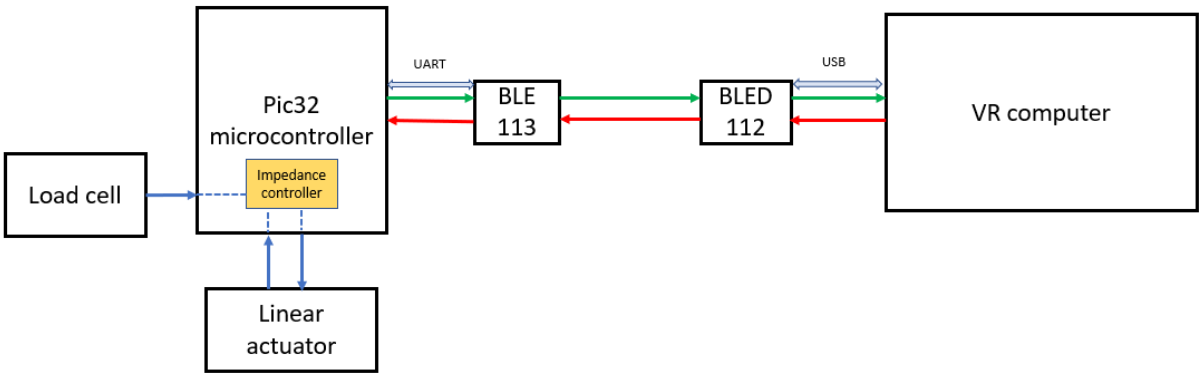

Figure 9. Bluetooth Data Flow. Finger position data are sampled from the linear actuator by the Pic32 microcontroller. These data are communicated to the BLE 113 over UART. The Bluetooth radio stack sends the data to BLED 112, which is connected as a USB dongle in the VR computer. The command issued from the VR computer to the Pic32 microcontroller is shown in red. On receiving the haptic command, the impedance controller programmed in Pic32 is executed. The impedance controller takes force and motor position as inputs and produces an analog signal between 0 – 5V that commands the actuator to the desired position.

3.3.2 Data Logging

The BLE link was also leveraged to send actual and desired force and motor position values from the Pic32 controller to compile in a csv (comma-separated values) file in the Unity platform. Other parameters like error, integrator, derivative, and PID terms, were also shared in the link for debugging purposes at a frequency of 10 Hz. These data are important for tracking user performance so that therapy can be adjusted accordingly to best meet the needs of the individual.

3.4 Haptic Feedback

Haptic feedback was implemented through an impedance controller. There are different types of impedance controller based on the types of force and position relationship being used, namely stiffness (position proportional), damping (velocity proportional), and general impedance (position, velocity, and acceleration proportional) [34]. Stiffness based impedance controller

was implemented in this study. The impedance controller can simulate different mechanical impedances at the end effector to applied forces. Different stiffness values were simulated to match different objects like a rubber ball, sponge block and eraser thus providing haptic feedback.

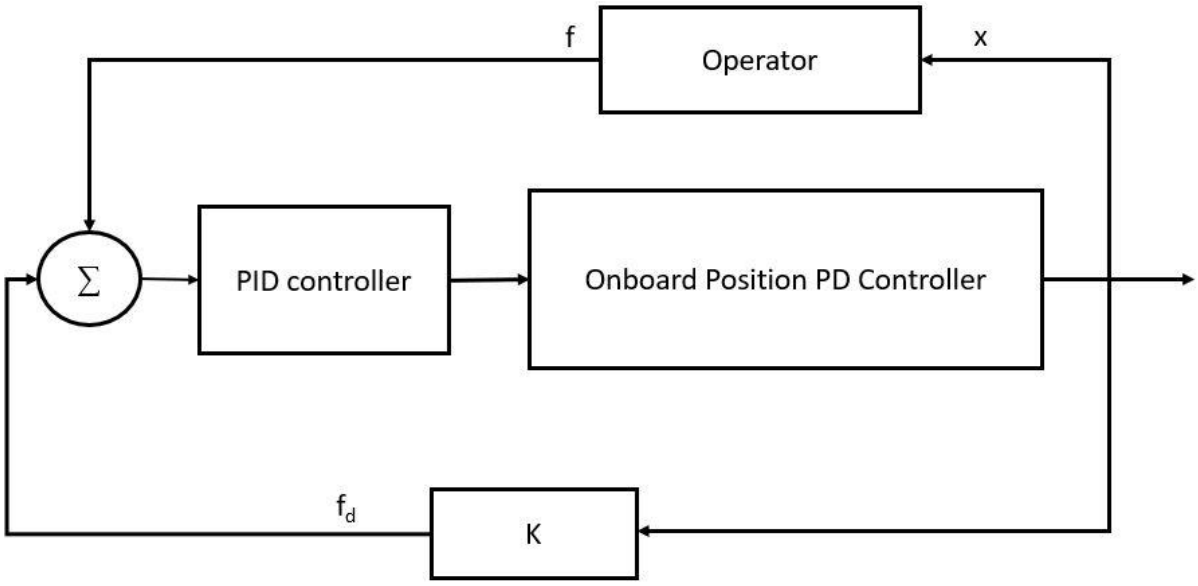

Figure 10. Block Diagram of Impedance controller. The controller maintains force delivered to the user by adjusting the position. Both force and position feedback were used, leading to the implementation of the impedance controller with force feedback.

3.4.1 PID Control

The objective of the PID controller is to translate force values to correct position input to maintain the desired force felt by the user. A digitized version of the PID controller was coded in the Pic32 microcontroller. Under this implementation, the integrator was assumed to act as an accumulator (**Eqn 3.4**) with clipping; and it was reset every 2 seconds to prevent overflow. The value of 2 seconds was found through trial and error method. Also, the derivative term was treated as the difference between previous and current error terms (**Eqn. 3.5**). The desired

position of the actuator x_d forms the input of the 12-bit DAC. The current position of the actuator is a 16-bit value. To calculate the desired position, the current position is mapped to a 12-bit value x and is subtracted by PID terms (**Eqn. 3.6**).

$$error = desired\ force - actual\ force \tag{3.3}$$

$$integrator\ +=\ error \tag{3.4}$$

$$derivative = error - previous\ error \tag{3.5}$$

$$x_d = x - (K_p error + K_i integrator + K_d derivative) \tag{3.6}$$

P, I, D gains (Kp, Ki, Kd respectively) were found using the Ziegler and Nichols tuning method. In this process, a small test signal of amplitude P was given to the system running in an open-loop, and its response was recorded (**Figure 11**). This open-loop reaction curve was analyzed to determine the reaction rate (R), lag(L) [35] to calculate PID constants as per Table 3 in the appendix.

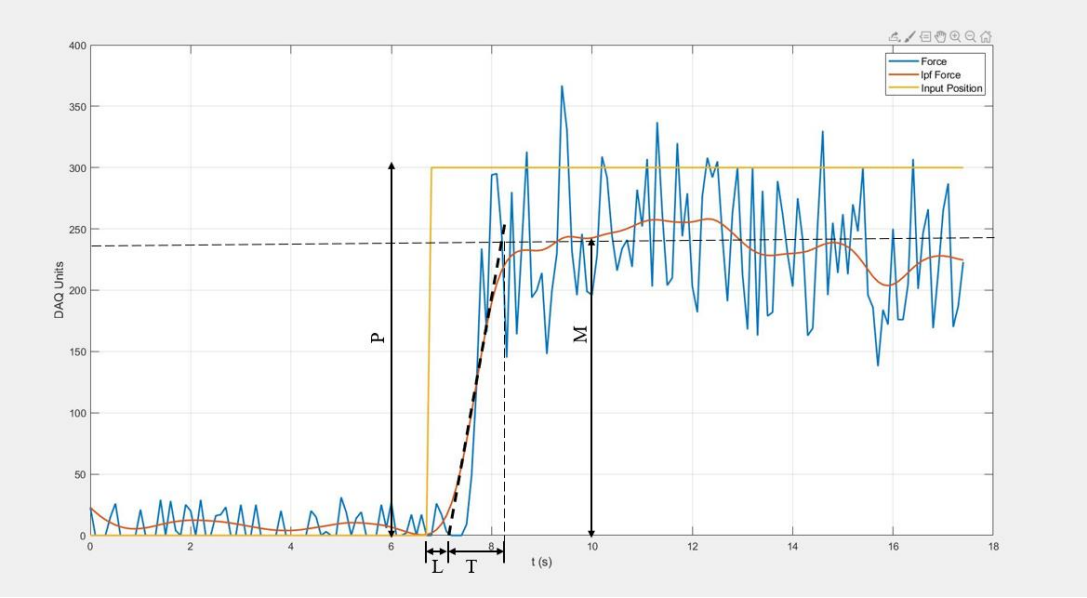

Figure 11. Open-loop control. Force response of the system was analyzed with a small input test signal. Reaction rate $R = M/T$.

Following the Table 5 (**Appendix A**), the constants for a P and a PID controller were calculated as below.

P controller : $K_p = 2.35$

PID controller : $K_p = 2.82$

$K_i = 2.82$

$K_d = 0.7$

These values were taken as a good initial values. Tuning of the values was then performed. For tuning, different force profiles like step, trapezoidal, sine waveforms were considered.

3.4.2 Stiffness Modulation

The stiffness K, of a sponge block, a rubber ball, and an eraser were determined to be 0.38 N/mm, 0.67 N/mm, and 2.26 N/mm, respectively [36]. The desired force of the controller f_d, is the product of stiffness and change in position Δx (**Eqn. 3.9**). When an object was picked up by the user, the VR game would save the length of the actuator as threshold position x_t. The current actuator position x and x_t were used to calculate the amount of 'penetration,' Δx (**Eqn. 3.7**). Linear relationships were used to convert between physical world quantities such as N, mm and $DAQ\ Counts$ (**Eqn. 3.8**), (**Eqn. 3.10**). Since the force calculations involved change in position, constant terms in the linear equation were neglected. The actual force produced by the glove is perceived as haptic feedback by the user.

$$\Delta x\ (DAQ\ Counts) = x - x_t \tag{3.7}$$

$$\Delta x\ (mm) = \Delta x\ (DAQ\ Counts) \times -0.0013 \tag{3.8}$$

$$f_d\ (N) = K \times \Delta x\ (mm) \tag{3.9}$$

$$f_d\ (DAQ\ Counts) = f_d\ (N) \times 251.46 + base\ force \tag{3.10}$$

The impedance controller was validated by plotting force and position data of the actuator. The slope of the graph was expected to match the stiffness value being simulated.

3.4.3 Validation Testing

Validation testing was first performed for a mockup of the exoskeleton finger and then for the exoskeleton itself. The mockup consisted of one linear actuator, which was supported on a magnetic base. The end of the shaft housed the load cell which was connected to a spring of stiffness 2 N/mm by a monofilament cable with a maximum tensile strength of 9 kg (**Figure 11**). It is assumed that each finger is a spring only system. One finger of the exoskeleton was then controlled by a glove in **Figure 1**.

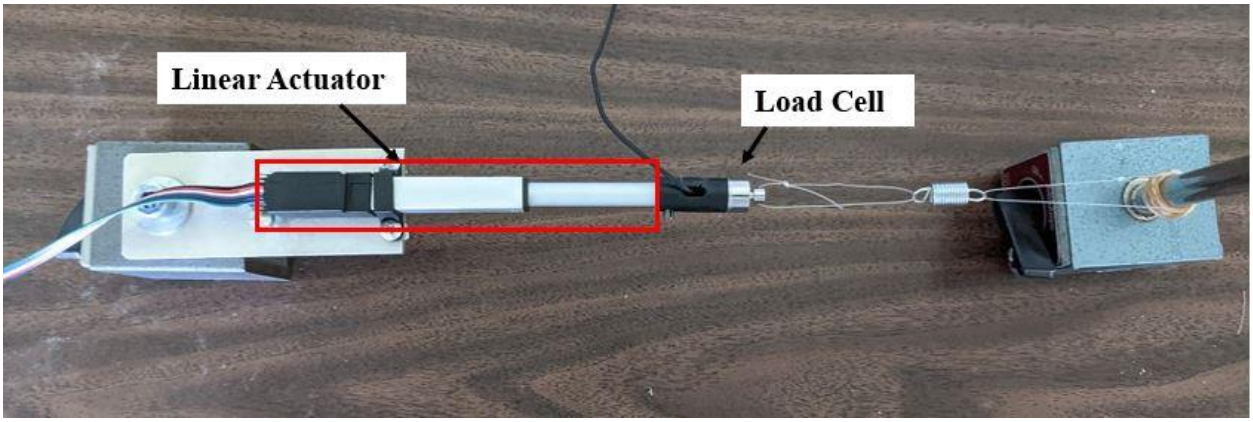

Figure 12. X-Glove actuator test setup. The system models actuation of one finger with the actuator, load cell, and other electrical components constituting the X-Glove.

CHAPTER 4: RESULTS AND DISCUSSION

4.1 Efficiency of PID vs. Proportional Controller

The PID controller was tested for its ability to track desired ramp and sinusoidal force profiles. Comparisons were made between a proportional (P) controller and the PID controller. The PID controller was expected to be better than the P controller in eliminating steady-state error and achieving a quicker response time. RMSE was calculated for the responses of the P and the PID controllers (**Table 3**). The PID controller had lower RMSE than the P controller for all force profiles (**Figure 13**) except for the sinusoidal force profile of 1 Hz. This exception is due to the limitation of the actuator. The actuator had a position PD controller. This position controller turned off the motor to prevent it from damage caused due to its oscillatory movement back and forth. While the P controller was able to achieve a good response, the PID controller was able to perform slightly better than the P controller (**Figure 14**).

Table 3. Comparison of P and PID Controller

Force Profile	RMSE of P controller (N)	RMSE of PID Controller (N)
A	4.8	4.56
B	0.89	0.63
C	0.69	0.54
D	0.51	0.49
E	0.96	0.51
F	0.44	0.41
G	9.99	10.91

Figure 13. Comparison between P and PID Controller. $K_p = 1$ for P controller. $K_p = 0.96$, $K_i = 0.001$, $K_d = 0.25$ for PID Controller. These constant values were chosen after analyzing the performance of the controller to different force profiles such as the step trajectory (A and B), trapezoidal trajectories of different ramps (C-H), and sinusoidal trajectories of different frequencies (I-N). Left column (A, C, E, G, I, K, M) were responses for the P controller. Similarly, right column (B, D, F, H, J, L, N) plots show responses for the PID controller.

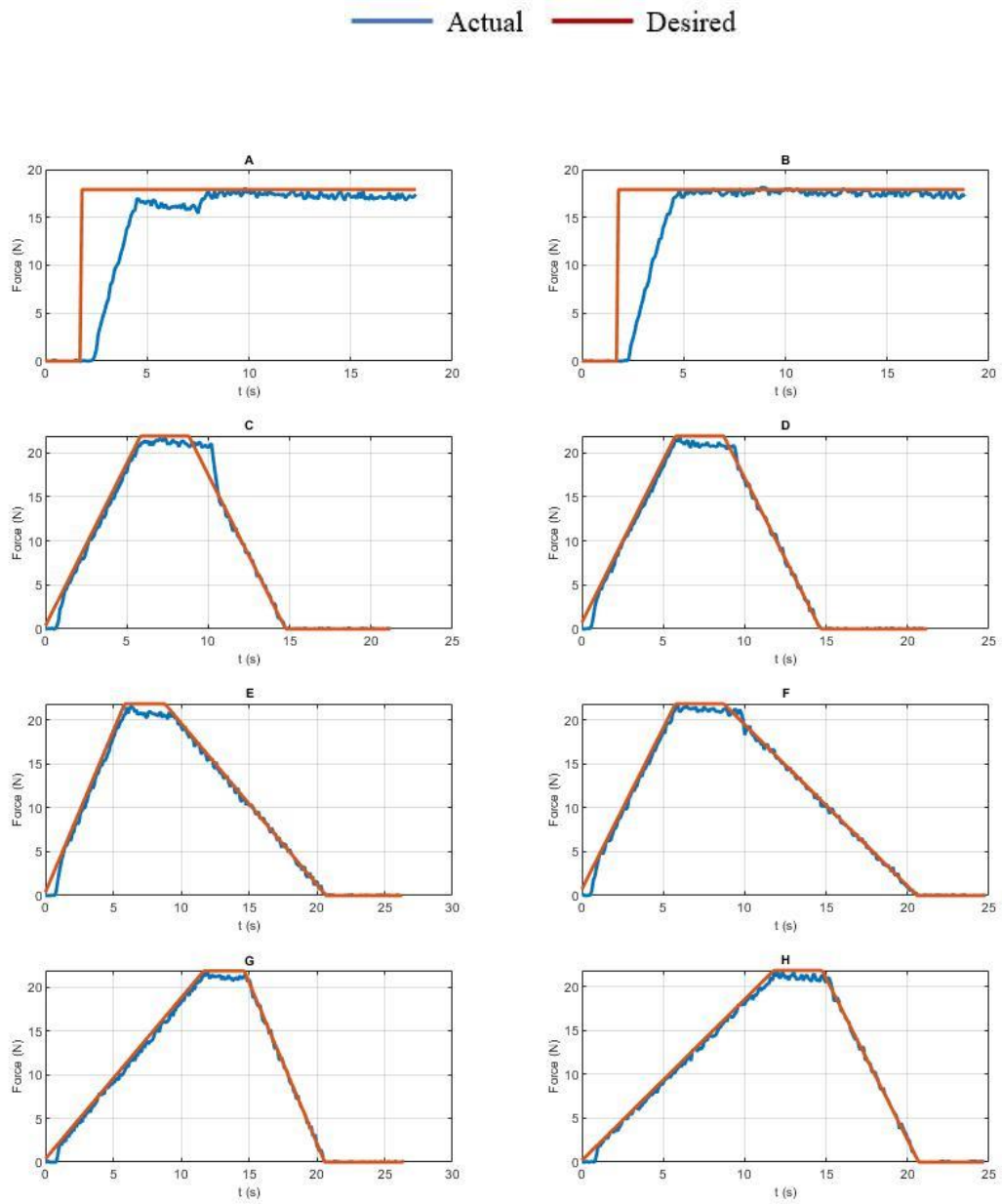
Actual
Desired
A
B
C
D
E
F
G
H
Force (N)
t (s)

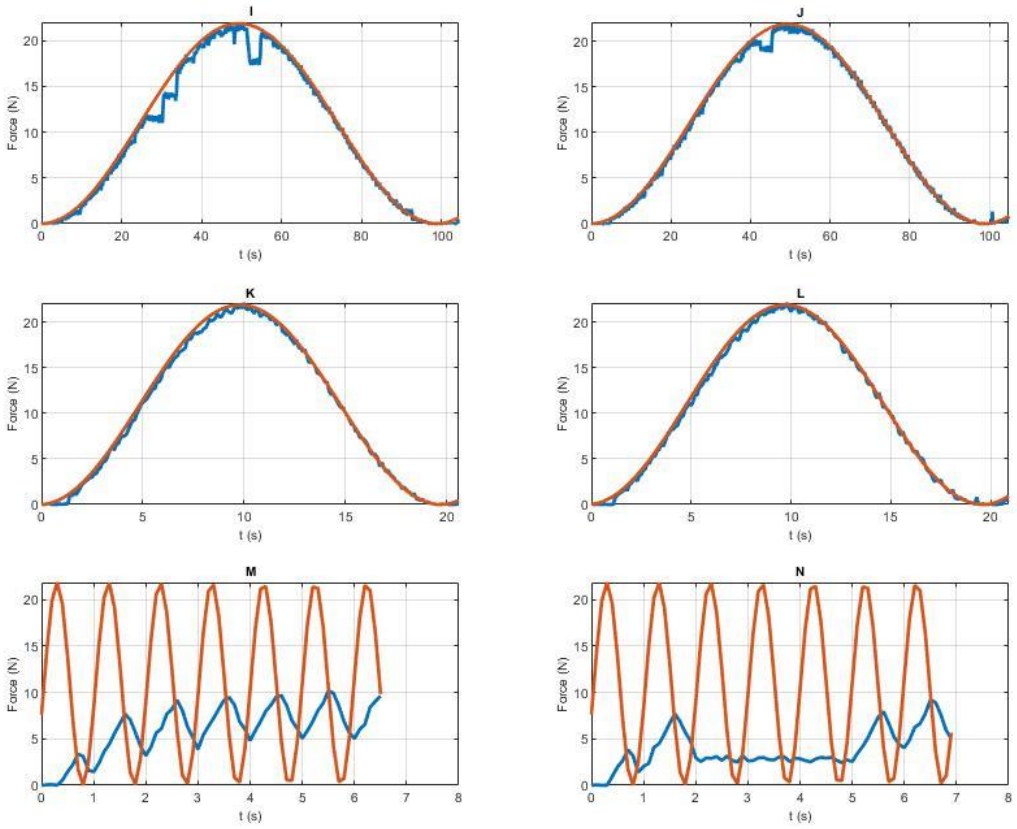
I
J
K
L
M
N
Force (N)
t (s)

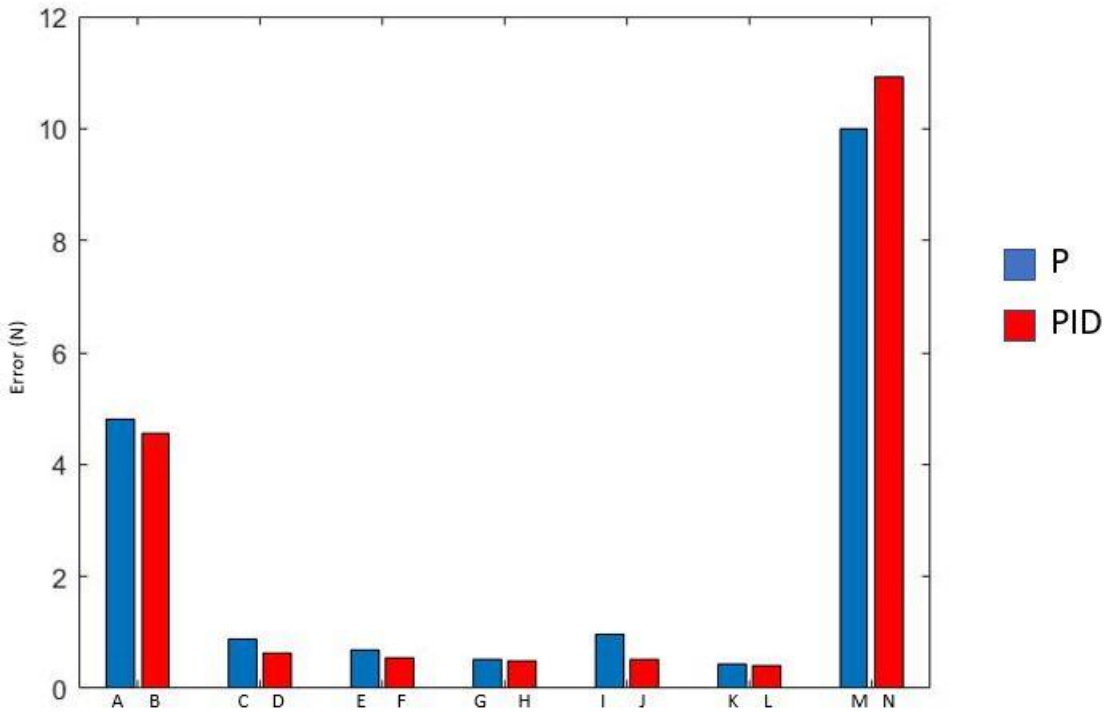

Figure 14. RMSE Comparison between P and PID Controller. RMSE values are grouped based on the input force profiles shown in **Figure 12**.

The Bode plot for the system was created by an experimental approach to find the frequency response of the system. Desired sinusoidal profiles of constant amplitude of 20 N and different frequencies were employed to evaluate the controller performance. Signal frequency was varied from 0.01 Hz to 2 Hz (0.01, 0.05, 0.067, 0.1, 0.2, 0.5, 1, 2), and the controller`s response was recorded. The P and PID controllers showed similar behavior, with the magnitude decreasing by -3 dB at approximately 0.375 Hz (**Figure 15 A**). This places an upper limit on the fingertip force frequency. When fingers undergo flexion and extension at a rate higher than 0.375 Hz, the actuator will not be able to respond well. The speed and the proprietary position controller of the motor might be the reasons behind the low bandwidth value.

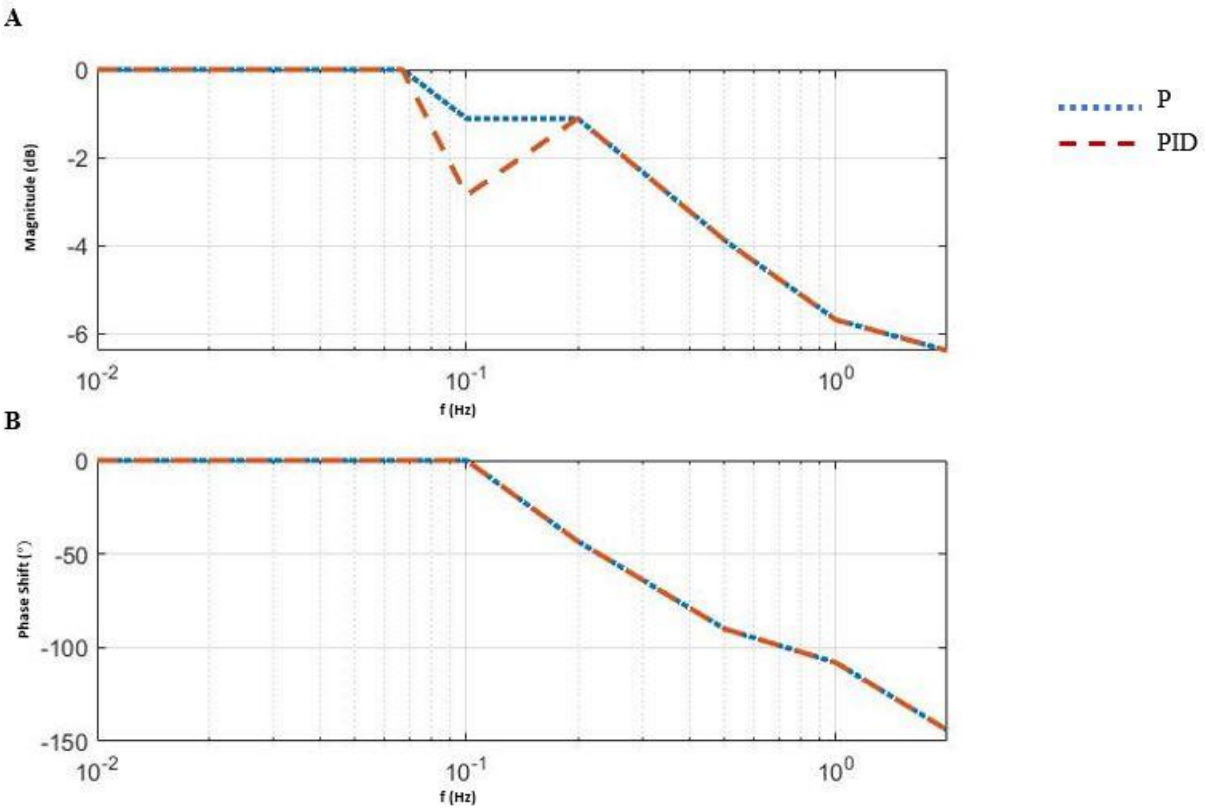

Figure 15. Bode plot. (A) The ratio of output to input amplitude is measured in decibels against the input frequencies. (B) The phase shift is plotted against the input sinusoidal frequencies. Both P and PID controllers have the same phase shift plot.

4.2 Stiffness Modulation

The performance of the impedance controller for the X-Glove was then evaluated for three stiffness values, 0.38 N/mm, 0.67 N/mm and 2.26 N/mm. Extension forces were manually applied to the motor shaft and the motor had to respond to simulate a different stiffness level, as shown in **Figure 16**. The efficiency of both P and PID controllers was evaluated by plotting force and distance data (**Figure 16**). In **Figure 16E & F)**. These figures show that the curve is linear only up to about 22 N of force. This is due to limitations in the force the motor can

produce in one direction while moving in the opposite direction. The actuator datasheet lists the maximum back drive force of the actuator, as 22 N as per the actuator datasheet.

The controllers were able to achieve the range of stiffness values tested. RMSE values for the PID controller were less than those for the P controller for all the three stiffness values. For a desired stiffness of 2.26 N/mm, both controllers could only provide the desired stiffness up to the limit of 22 N, due to the limitations of the motor. Hence, only the linear region was used for RMSE calculation (**Table 4**). The RMSE of both the controllers increased with stiffness value. However, the RMSE of the PID controller was less than that of P controller by 87% for the highest stiffness value in this study (2.26 N/mm) and by 35% for K = 0.38 N/mm. Hence, the PID controller is desirable despite the stiffness values.

Table 4. RMSE values for different stiffness values

Stiffness *K* (N/mm)	**P controller RMSE (N)**	**PID controller RMSE (N)**
0.38	0.51	0.33
0.67	1.56	0.35
2.26	5.86	0.76

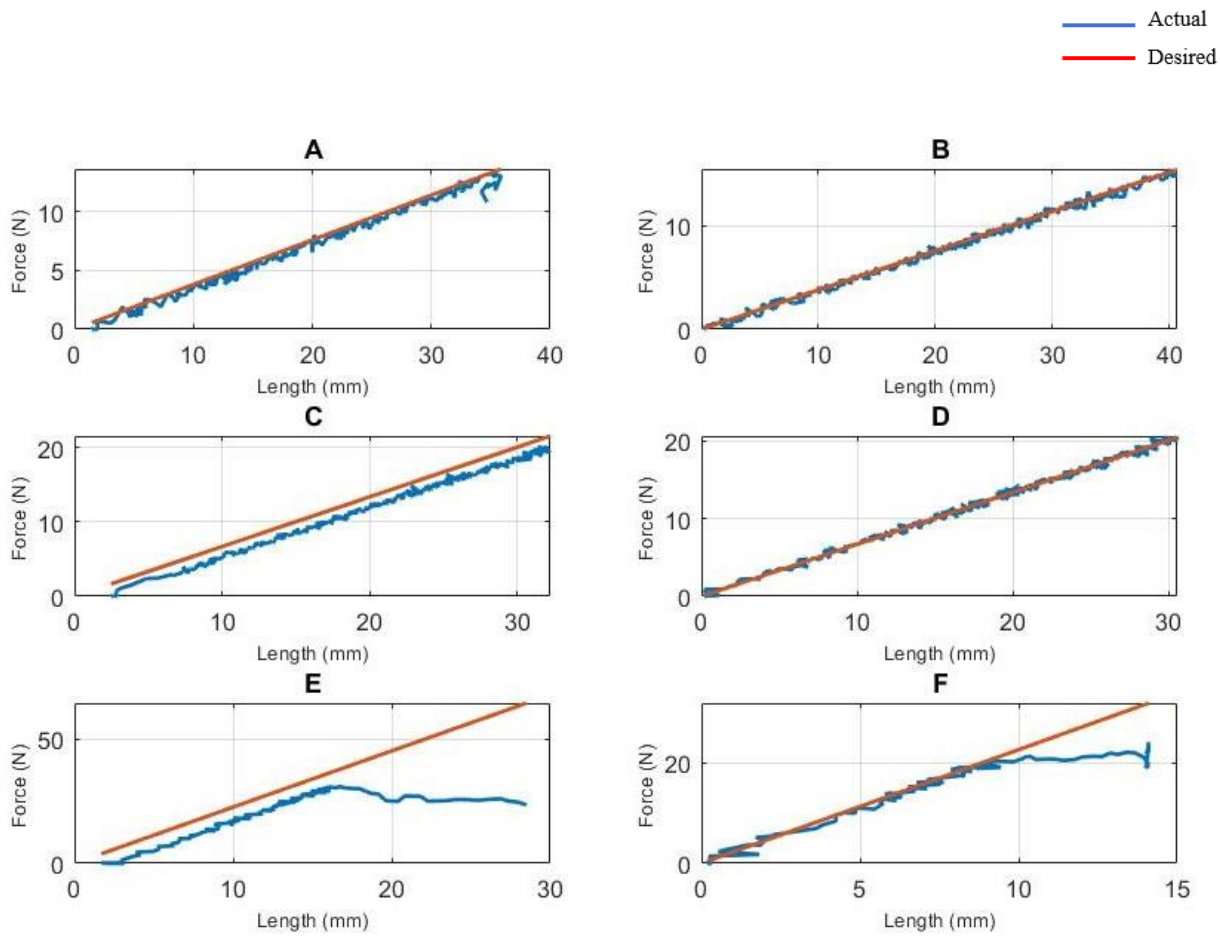

Figure 16. Stiffness curves. Graphs (A), (C), (E) are showing the performance of P controller with different stiffness values such as 0.38 N/mm, 0.67 N/mm, and 2.26 N/mm, respectively. Graphs (B), (D), (F) are the stiffness curves of the PID Controller with stiffness values such as 0.38 N/mm, 0.67 N/mm, and 2.26 N/mm, respectively. Values were recorded by pulling the motor shaft out, increasing the distance. As the distance increases, it can be seen that the force increases too.

4.3 Communication

The BLE system proved effective for communicating between the X-Glove and VR computer. For a baud rate of 115200, zero command misses from the VR computer to the X-Glove were observed. During the course of the study, there were a very few instances during which the Bluetooth modules were unable to connect. Restarting the bluetooth connection in the VR game scene solved the issue.

The round-trip time for sending a command from the X-Glove controller to the VR game scene, processing the signal in the game and then sending back commands to the X-Glove controller took a maximum of 142 ms and a minimum of 52 ms. This is based on the assumption that time taken to toggle general purpose input output (GPIO) pins in Pic32 is negligible. This delay is not a limiting factor as the X-Glove itself has a bandwidth of 0.375 Hz.

CHAPTER 5: CONCLUSION

The objective of this study was to implement haptic feedback for the virtual reality therapy by incorporating the X-Glove exoskeleton. An impedance controller was chosen to implement the haptic feedback. The feasibility of providing visual feedback was also explored through a mesh deformation technique.

5.1 Control of Haptic Feedback

Force in the system was controlled indirectly by a PID controller, which controls the position of the actuator. The PID controller exhibited superior performance to the P controller in terms of accuracy and robustness at lower stiffness values. At larger stiffness values, both controllers had similar RMSE values. The onboard (nonprogrammable) position PD controller for the servomotor played a predominant role in the rise time. Hence, even with the PID controller with the best gains, there was still a lag of 0.4 seconds. This onboard PD controller is also believed to have impacted performance due to its safety circuits. Namely, the motor would turn off during constant or oscillatory inputs. The actuator exhibited different stiffness values for push or pull operations, thus demonstrating to provide haptic feedback for the user. The maximum bandwidth for force tracking was 0.375 Hz. For the intended application, however, this bandwidth should be sufficient. Rapid finger joint movement can evoke an undesired spastic stretch reflex in stroke survivors [37].

5.2 Limitations

Delayed response time and uncertainty of the actuator are limitations in this study. The controller for the chosen linear actuator was proprietary and had limitations. The motor behaved randomly under certain circumstances. This effect was noticed in both PID and P controller when they were being assessed with trapezoidal (**Figure 17**) and sinusoidal force profile (**Figure**

18). In a trapezoidal force profile with a maximum desired force of 20 N, the actuator failed to reach the maximum force in random trials. It was accompanied by a lag while tracking the ramp-down part of the force profile. In a sinusoidal profile of 2 Hz frequency, the actuator was expected to oscillate with lesser amplitude than the input and with a phase difference. However, the actuator stopped oscillating at a random period in the trial.

Though the PID or P controller issued motor position commands, the position PD controller in the actuator has the ultimate control of positioning the actuator. The non-programmable settings of the PD controller are believed to turn off the motor when issued motor position commands are within a threshold range as in trapezoidal profile and during oscillations in sinusoidal profile to prevent the motor from damage [38]. This is the likely reason for uncertainty in the system response.

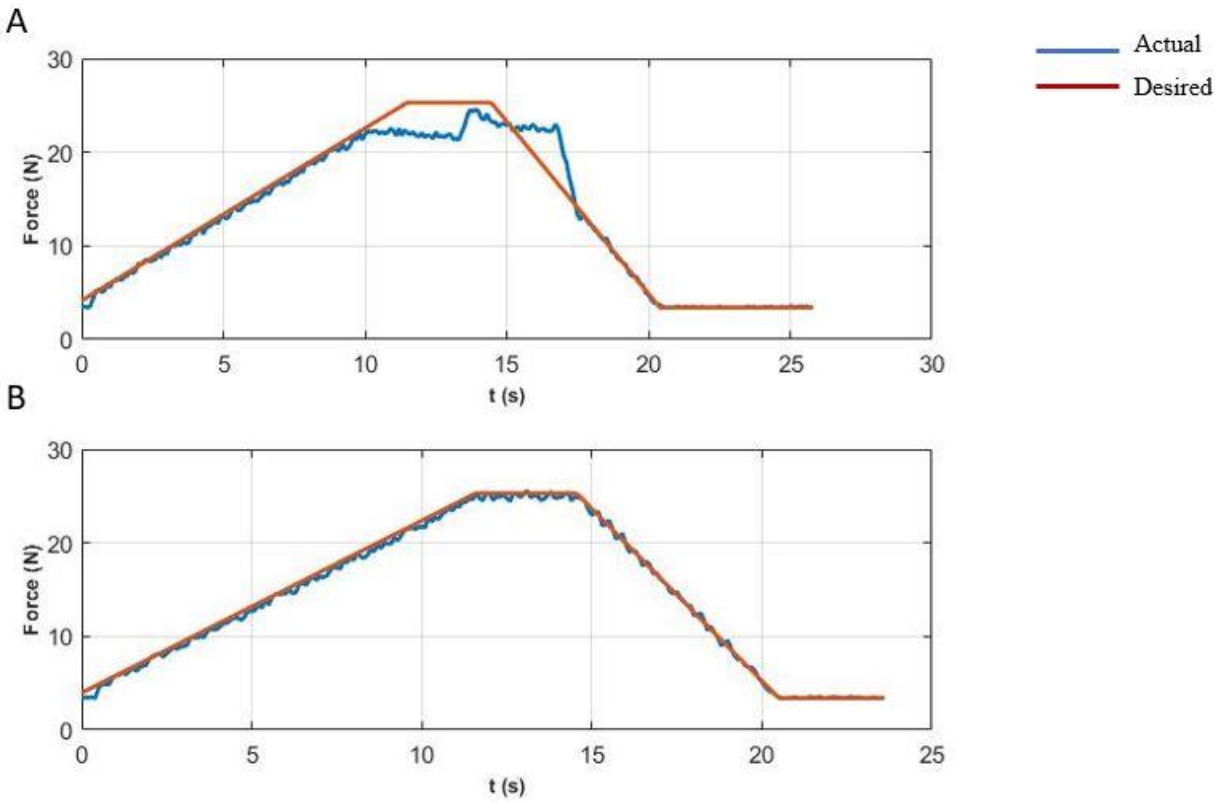

Figure 17. Randomness in trapezoidal profile. Sometimes, a lag is found in the transition from constant to ramp-down state in different trials of the same experiment.

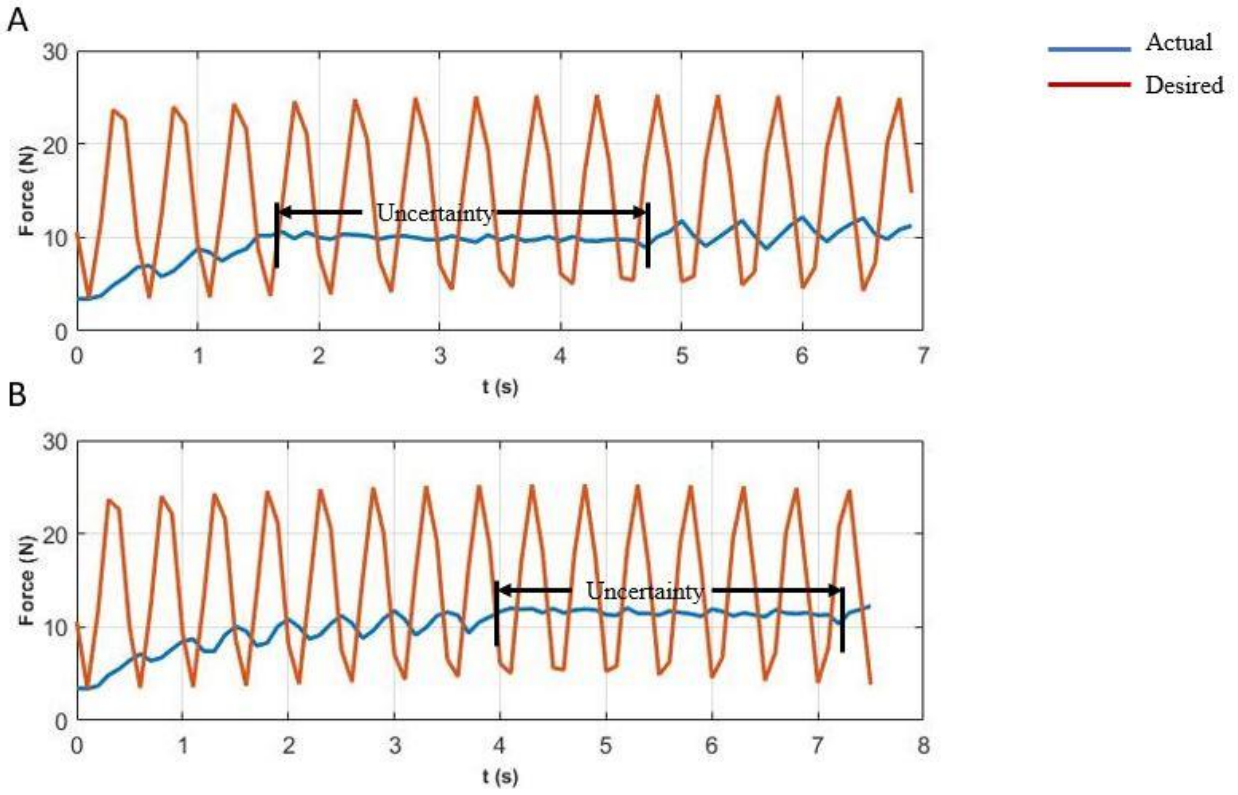

Figure 18. Randomness in sinusoidal profile. The system was excited with sinusoidal input of 2 Hz frequency, and its response was recorded for two trials. The actuator is turned off randomly at different periods in the trials.

5.3 Future Directions

The next step of the project might be to test the haptic feedback with the X-Glove by expanding to utilizing all 5 digits. Mesh deformation might be applied to objects in the game scene. After that, the haptic feedback could be tested with neurologically intact persons and could be followed by assessing it in the stroke survivors. Finally, it could be deployed in home based rehabilitation and the benefits of using haptics could be assessed.

REFERENCES

[1] D. Tsoupikova, K. Triandafilou, K. Thielbar, G. Rupp, F. Preuss, and D. Kamper, "Multi-user virtual reality therapy for post-stroke hand rehabilitation at home," *7th Int. Multi-Conference Complexity, Informatics Cybern. IMCIC 2016 7th Int. Conf. Soc. Inf. Technol. ICSIT 2016 - Proc.*, vol. 1, no. 2, pp. 227–231, 2016.

[2] K. M. Triandafilou, D. Tsoupikova, A. J. Barry, K. N. Thielbar, N. Stoykov, and D. G. Kamper, "Development of a 3D, networked multi-user virtual reality environment for home therapy after stroke," *J. Neuroeng. Rehabil.*, vol. 15, no. 1, pp. 1–14, 2018.

[3] M. A. Guadagnoll and T. D. Lee, "Challenge Point: A Framework for Conceptualizing the Effects of Various Practice Conditions in Motor Learning," *J. Mot. Behav.*, vol. 36, no. 2, pp. 212–224, 2004.

[4] A. K. Welmer, L. W. Holmqvist, and D. K. Sommerfeld, "Limited fine hand use after stroke and its association with other disabilities," *J. Rehabil. Med.*, vol. 40, no. 8, pp. 603–608, 2008.

[5] E. J. Benjamin *et al.*, *Heart disease and stroke statistics - 2018 update: A report from the American Heart Association*, vol. 137, no. 12. 2018.

[6] "American Stroke Assosciation." [Online]. Available: https://www.stroke.org/en/about-stroke.

[7] E. J. Benjamin *et al.*, *Heart Disease and Stroke Statistics'2017 Update: A Report from the American Heart Association*, vol. 135, no. 10. 2017.

[8] "National Institute of Neurological Disorders and Stroke." [Online]. Available: https://www.stroke.nih.gov/materials/rehabilitation.htm.

[9] H. Nakayama, H. Stig Jørgensen, H. Otto Raaschou, and T. Skyhøj Olsen, "Recovery of

upper extremity function in stroke patients: The Copenhagen stroke study," *Arch. Phys. Med. Rehabil.*, vol. 75, no. 4, pp. 394–398, 1994.

[10] D. G. Kamper, H. C. Fischer, E. G. Cruz, and W. Z. Rymer, "Weakness Is the Primary Contributor to Finger Impairment in Chronic Stroke," *Arch. Phys. Med. Rehabil.*, vol. 87, no. 9, pp. 1262–1269, 2006.

[11] J. J. Gemperline, S. Allen, D. Walk, and W. Z. Rymer, "Characteristics of motor unit discharge in subjects with hemiparesis," *Muscle Nerve*, vol. 18, no. 10, pp. 1101–1114, 1995.

[12] G. Hoffmann, M. O. Conrad, D. Qiu, and D. G. Kamper, "Contributions of voluntary activation deficits to hand weakness after stroke," *Top. Stroke Rehabil.*, vol. 23, no. 6, pp. 384–392, 2016.

[13] S. W. Lee, K. Triandafilou, B. A. Lock, and D. G. Kamper, "Impairment in Task-Specific Modulation of Muscle Coordination Correlates with the Severity of Hand Impairment following Stroke," *PLoS One*, vol. 8, no. 7, 2013.

[14] N. J. Seo, W. Z. Rymer, and D. G. Kamper, "Altered digit force direction during pinch grip following stroke," *Exp. Brain Res.*, vol. 202, no. 4, pp. 891–901, 2010.

[15] D. G. Kamper and W. Z. Rymer, "Impairment of voluntary control of finger motion following stroke: Role of inappropriate muscle coactivation," *Muscle and Nerve*, vol. 24, no. 5, pp. 673–681, 2001.

[16] M. D. Rinderknecht *et al.*, "Reliability, validity, and clinical feasibility of a rapid and objective assessment of post-stroke deficits in hand proprioception," *J. Neuroeng. Rehabil.*, vol. 15, no. 1, pp. 1–16, 2018.

[17] R. S. Johansson, "Sensory Control of Dexterous Manipulation in Humans," *Hand Brain*,

pp. 381–414, 1996.

[18] C. J. Winstein *et al., Guidelines for Adult Stroke Rehabilitation and Recovery: A Guideline for Healthcare Professionals from the American Heart Association/American Stroke Association*, vol. 47, no. 6. 2016.

[19] J. Young and A. Forster, “Day hospital and home physiotherapy for stroke patients: a comparative cost-effectiveness study.,” *J. R. Coll. Physicians Lond.*, vol. 27, no. 3, pp. 252–258, 1993.

[20] Diering, “乳鼠心肌提取 HHS Public Access,” *Physiol. Behav.*, vol. 176, no. 1, pp. 139–148, 2018.

[21] H. J. Sung *et al.*, “Cortical reorganization and associated functional motor recovery after virtual reality in patients with chronic stroke: An experimenter-blind preliminary study,” *Arch. Phys. Med. Rehabil.*, vol. 86, no. 11, pp. 2218–2223, 2005.

[22] A. Turolla *et al.*, “Virtual reality for the rehabilitation of the upper limb motor function after stroke: A prospective controlled trial,” *J. Neuroeng. Rehabil.*, vol. 10, no. 1, pp. 1–9, 2013.

[23] L. Piron, P. Tonin, F. Piccione, V. Iaia, E. Trivello, and M. Dam, “Therapy for Arm Motor,” *Methods*, vol. 14, no. 6, pp. 732–740, 2002.

[24] K. Laver, S. George, J. Ratcliffe, and M. Crotty, “Virtual reality stroke rehabilitation - hype or hope?,” *Aust. Occup. Ther. J.*, vol. 58, no. 3, pp. 215–219, 2011.

[25] J. A. Kleim and T. A. Jones, “Principles of experience-dependent neural plasticity: Implications for rehabilitation after brain damage,” *J. Speech, Lang. Hear. Res.*, vol. 51, no. 1, 2008.

[26] G. Saposnik and M. Levin, “Virtual reality in stroke rehabilitation: A meta-analysis and

implications for clinicians," *Stroke*, vol. 42, no. 5, pp. 1380–1386, 2011.

[27] D. M. Vo, J. M. Vance, and M. G. Marasinghe, "Assessment of haptics-based interaction for assembly tasks in virtual reality," *Proc. - 3rd Jt. EuroHaptics Conf. Symp. Haptic Interfaces Virtual Environ. Teleoperator Syst. World Haptics 2009*, pp. 494–499, 2009.

[28] A. Turolla *et al.*, "Haptic-based neurorehabilitation in poststroke patients: A feasibility prospective multicentre trial for robotics hand rehabilitation," *Comput. Math. Methods Med.*, vol. 2013, 2013.

[29] J. C. Metzger, O. Lambercy, A. Califfi, F. M. Conti, and R. Gassert, "Neurocognitive robot-assisted therapy of hand function," *IEEE Trans. Haptics*, vol. 7, no. 2, pp. 140–149, 2014.

[30] L. Jiang, M. R. Cutkosky, J. Ruutiainen, and R. Raisamo, "Using haptic feedback to improve grasp force control in multiple sclerosis patients," *IEEE Trans. Robot.*, vol. 25, no. 3, pp. 593–601, 2009.

[31] H. C. Fischer *et al.*, "Use of a Portable Assistive Glove to Facilitate Rehabilitation in Stroke Survivors with Severe Hand Impairment," *IEEE Trans. Neural Syst. Rehabil. Eng.*, vol. 24, no. 3, pp. 344–351, 2016.

[32] "Catlikecoding.com." [Online]. Available: https://catlikecoding.com/unity/tutorials/mesh-deformation/.

[33] K. Stock, "No Title." [Online]. Available: https://www.patreon.com/posts/26979494.

[34] A. S. Sadun, J. Jalani, and J. A. Sukor, "An overview of active compliance control for a robotic hand," *ARPN J. Eng. Appl. Sci.*, vol. 11, no. 20, pp. 11872–11876, 2016.

[35] J. G. Ziegler and N. B. Nichols, "Optimum settings for automatic controllers," *J. Dyn. Syst. Meas. Control. Trans. ASME*, vol. 115, no. 2B, pp. 220–222, 1993.

[36] S. Jeon and S. Choi, “Haptic augmented reality: Taxonomy and an example of stiffness modulation,” *Presence Teleoperators Virtual Environ.*, vol. 18, no. 5, pp. 387–408, 2009.

[37] D. G. Kamper and W. Z. Rymer, “Quantitative features of the stretch response of extrinsic finger muscles in hemiparetic stroke,” *Muscle and Nerve*, vol. 23, no. 6, pp. 954–961, 2000.

[38] L. Actuator and C. Board, “(Linear Actuator Control Board).”

APPENDICES

Appendix A

Ziegler and Nichols Tuning Chart

Control Mode	**K_p**	**T_i**	**T_d**
P	P/RL		
PI	0.9 P/RL	3.33L	
PID	1.2 P/RL	2L	0.5L

APPENDIX B

Jelly Physics

$$F_v = \frac{F}{1 + d^2}$$

$$a = \frac{F}{m}$$

All vertices are considered of uniform mass. Hence, acceleration a at each vertex is given by

$$a = F_v$$

$$a = \frac{v}{\Delta t}$$

$$v = F_v \, \Delta t$$

Adding spring force, vertex velocity is reduced as

$$v \mathrel{-}= (\Delta x \times Spring\ constant \times \Delta t)$$

To prevent eternal oscillation, this velocity is multiplied by damping factor d as

$$v \mathrel{*}= (1 - d\Delta t)$$